Title

Self-Healing and Anti-CO2 Hydrogels for Flexible Solid-State Zinc-Air Batteries

Journal

ACS Applied Materials & Interfaces, 13(10)

ISSN

1944-8244

Authors

Zhao, Siyuan
Xia, Dawei
Li, Minghao
et al.

Publication Date

2021-03-17

DOI

10.1021/acsami.1c00012

Peer reviewed

Self-Healing and Anti-CO_2 Hydrogels for Flexible Solid-State Zinc-Air Batteries

Siyuan Zhao, Dawei Xia, Minghao Li, Diyi Cheng, Keliang Wang, Ying Shirley Meng, Zheng Chen,* and Jinhye Bae*

ABSTRACT: Flexible solid-state zinc-air batteries (ZABs) generally suffer from poor electrolyte/electrode contact and mechanical degradation in practical applications. In addition, CO_2 corrosion is also a common issue for ZABs with alkaline electrolyte. Herein, we report a thermoreversible alkaline hydrogel electrolyte that can simultaneously solve the aforementioned problems. Through a simple cooling process, the hydrogel electrolyte transforms from solid state to liquid state that can not only restore the deformed electrolyte layer to its original state but also rebuild intimate contact between electrode and electrolyte. Moreover, the ZAB based on this hydrogel electrolyte exhibits an unprecedented anti-CO_2 property. As a result, such a battery shows almost 2.5 times discharge duration than that of ZAB based on liquid electrolyte.

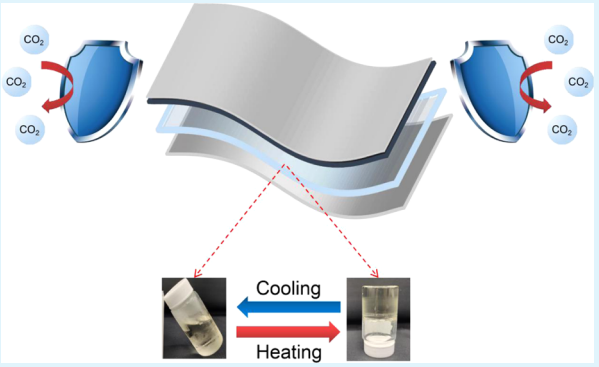

KEYWORDS: *zinc-air battery, hydrogel electrolyte, thermoreversible gel, CO_2 corrosion, self-healing, electrode/electrolyte interface*

INTRODUCTION

With the rapid development of wearable electronic devices, flexible solid-state aqueous batteries have emerged as promising power sources owing to their superior safety and low cost.[1−3] Among them, zinc-air battery (ZAB) is particularly attractive due to its stable discharging voltage and high theoretical energy density (1084 Wh/kg), which is about 4 times higher than that of lithium-ion battery (LIB).[4−6] Meanwhile, the worldwide abundant zinc reserves guarantee a fairly low price for ZABs toward commercialization. To enable the flexibility of ZAB, the key is to develop a suitable solid-state electrolyte to replace the conventional potassium hydroxide (KOH) liquid electrolyte.[7,8]

Various solid-state electrolytes for ZAB, mainly hydrogels and alkaline anion-exchange membranes, have recently been reported to realize different flexible designs such as being stretchable, compressible, and bendable.[9−13] However, to date, there are still many issues that need to be addressed on solid-state electrolytes for ZAB. First, most solid-state electrolytes can be easily damaged by various deformation during daily use, resulting in deterioration of electrochemical performance. A very few studies have reported self-healable solid-state electrolytes,[14,15] which relies on manual interruption to restore mechanically damaged electrolytes in the assembled cells to achieve healing function. Second, since the ZAB is a semiopen system, the alkaline electrolyte will inevitably react with CO_2 in the air during the operation period, leading to a decrease in ionic conductivity.[5,16] In the existing research, there is no effective method to slow down the reaction between alkaline electrolyte and CO_2. In addition, the poor wetting along the solid−solid interface causes poor contact between solid-state electrolytes and electrodes.[17] Therefore, it is of great importance to develop a solid-state electrolyte with functions of self-recovery, anti-CO_2, and intimate contact with electrodes.

Herein, we report a thermoreversible hydrogel electrolyte, which can effectively solve the problems including poor electrolyte/electrode contact, mechanical degradation, and CO_2 corrosion of ZAB. The novel hydrogel electrolyte is a mixture of KOH solution and poly(ethylene oxide)$_{100}$−poly(propylene oxide)$_{65}$−poly(ethylene oxide)$_{100}$ (PEO_{100}−PPO_{65}−PEO_{100}, also known by the trade name Pluronic F127, abbreviated as F127), where KOH solution provides conductive hydroxide ions and F127 imparts electrolyte a cooling-recovery property. By a simple cooling process, not only the damaged electrolyte can restore to its original state but also the electrolyte/electrode interface is able to rebuild its intimate contact. It is also worth mentioning that the F127-KOH electrolyte showed a significantly improved CO_2

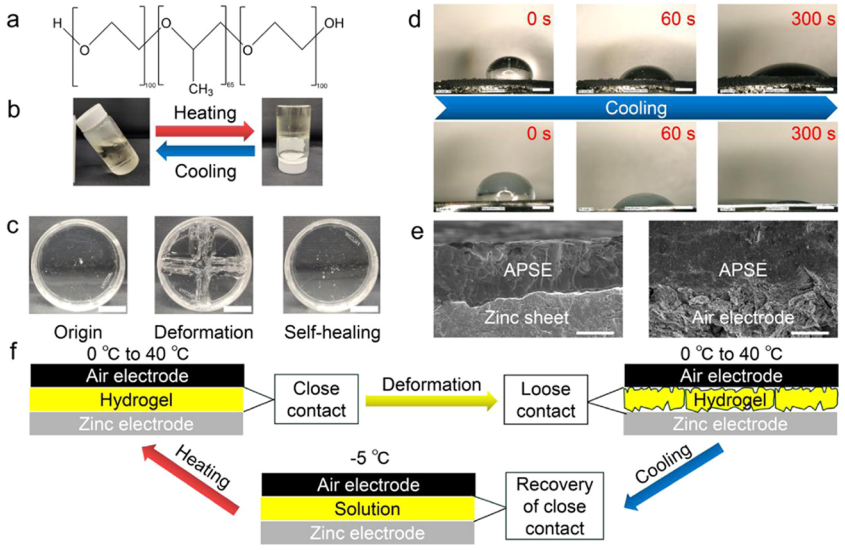

Figure 1. (a) Chemical structure of Pluronic F127. (b) Reversible sol−gel transition behavior of APSE. (c) Self-healing property of APSE. Scale bar: 1 cm. (d) Wetting process of the APSE on the air electrode (top row) and zinc electrode (bottom row), respectively, in a −5 °C environment. Scale bar: 100 μm. (e) Close contact between APSE and zinc/air electrode shown by cross-sectional SEM images. Scale bar: 20 μm. (f) Schematic of APSE-based ZAB's unique working process (close contact → loose contact → recovery of close contact).

resistance compared to the conventional KOH liquid electrolyte.

RESULTS AND DISCUSSION

F127 is a triblock copolymer (PEO_{100}−PPO_{65}−PEO_{100}), and the simplified structure of F127 is shown in Figure 1a. As a representative thermoreversible hydrogel, F127 endows its aqueous solution with a unique sol−gel transition property that exhibits a liquid state at a low temperature (e.g., <0 °C) and returns to a hydrogel state after heating. Although the mechanism of this phenomenon remains a controversial argument so far,[18] it is commonly considered that both the PEO and PPO blocks are hydrated with abundant water molecules through hydrogen bonding, hence well dissolved in water at a low temperature. However, at room temperature, PPO blocks gradually dehydrate and molecular aggregation of hydrophobic PPO blocks takes place. The aggregation of the PPO blocks leads to the formation of micelles, and eventually, the system becomes a gel by micelles packing.[19] The sol−gel transition is a physical process with no change in chemical components.[20]

The sol−gel transition temperature of the F127 solution is determined by the concentration of F127,[21] which is important for solid-state ZAB since a lower transition temperature (e.g., 0 °C) means a wider solid-state operating temperature range. The concentrations of F127 in deionized water and the corresponding transition temperatures were recorded (Table S1). The result exhibited a trend that with the increase of F127 solution wt %, the sol−gel transition temperature decreases, which is consistent with previous reports.[22] Except for this, the concentration of KOH also needs to be taken into consideration. For example, 6 M KOH solution has been widely used as an electrolyte for conventional ZAB due to its high ionic conductivity.[23] However, when it is applied in solid-state electrolytes, some polymer substrates, such as F127, are unable to endure alkaline solution with a high concentration. In other words, F127 powders could not dissolve in 6 M or even 1 M KOH solution completely (Figure S1). Accordingly, we optimized the concentration of KOH solution to 0.5 M, where the F127 powders completely dissolved in 0.5 M KOH solution and the sol−gel transition property of this mixture solution was maintained. In addition, we found that the existence of hydroxide ions (OH^-) significantly reduced the sol−gel transition temperature of F127 alkaline solution (12 °C for 30 wt % F127 in deionized water and −2 °C for 30 wt % F127 in 0.5 M KOH solution, Table S2). This phenomenon may provide a new aspect to explain the unique characteristic of Pluronic. Also, the freezing point of the new Pluronic hydrogel electrolyte dropped significantly by the effect of the KOH solution (Table S2). Hence, 0.5 M KOH solution and 30 wt % F127 were chosen as an optimized recipe for the alkaline Pluronic solid-state electrolyte (APSE) in this report.

APSE not only provides a large number of OH^- for ion transport but also maintains a cooling-recovery ability. As shown in Figure 1b, APSE can reversibly switch between liquid and hydrogel states through cooling and heating, respectively. Even if the surface of APSE is damaged or even cut into several parts, a simple cooling to −5 °C will turn APSE into a liquid and restore to its original state at room temperature (Figure 1c). From this perspective, APSE will maintain the advantage of intimate electrolyte/electrode contact like liquid-based ZAB because of its unique liquid state at a low temperature (−5 °C). Figure 1d exhibits the perfect wetting process of the zinc electrode and air electrode, respectively. Although the hydrogel-state APSE droplet had a relatively large contact angle at the beginning, it gradually became a liquid state at −5 °C, and thus spread spontaneously on the surface of both electrodes within 5 min. The cross-sectional scanning electron microscopy (SEM) images (Figure 1e) depict intimate contacts between APSE and both electrodes. There was no void observed at the electrolyte/electrode interface as a result of sufficient and complete infiltration of liquid-state APSE. Figure 1f illustrates the summary of the unique properties of APSE-based ZAB. Specifically, there is no obvious difference between the conventional flexible battery and the APSE-based ZAB in normal working environment. However, once APSE suffered from local stress or other kinds of deformations (e.g., crumbling and twisting), a low-temperature (−5 °C) stimulus

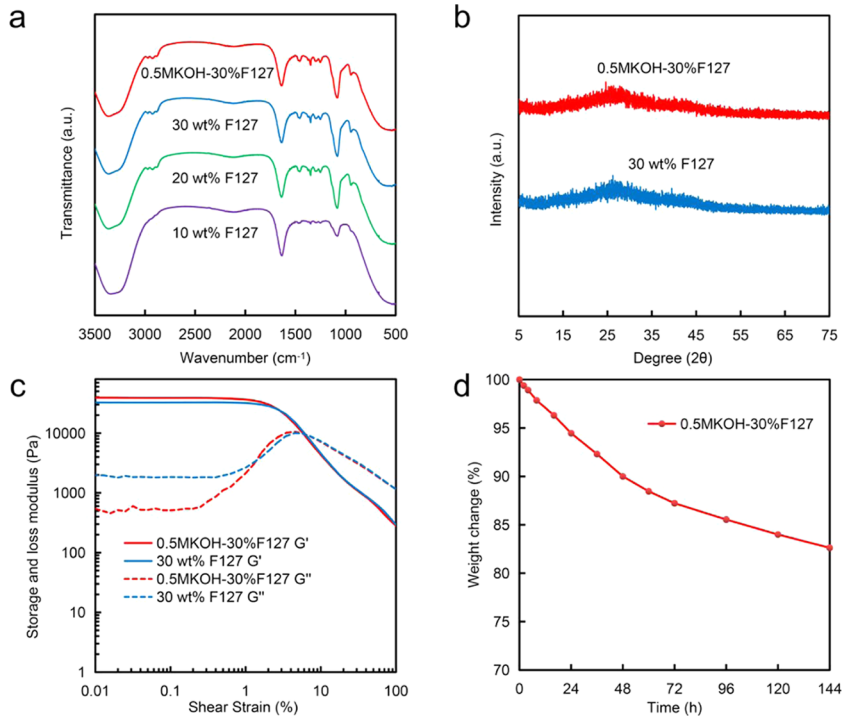

Figure 2. (a) FTIR spectra of APSE and Pluronic F127 with 10, 20, and 30 wt % concentrations. (b) XRD pattern of APSE and 30 wt % Pluronic F127. (c) Rheological behaviors of APSE and 30 wt % Pluronic F127, where G' represents the storage modulus and G'' represents the loss modulus. (d) Water retention capacity of APSE.

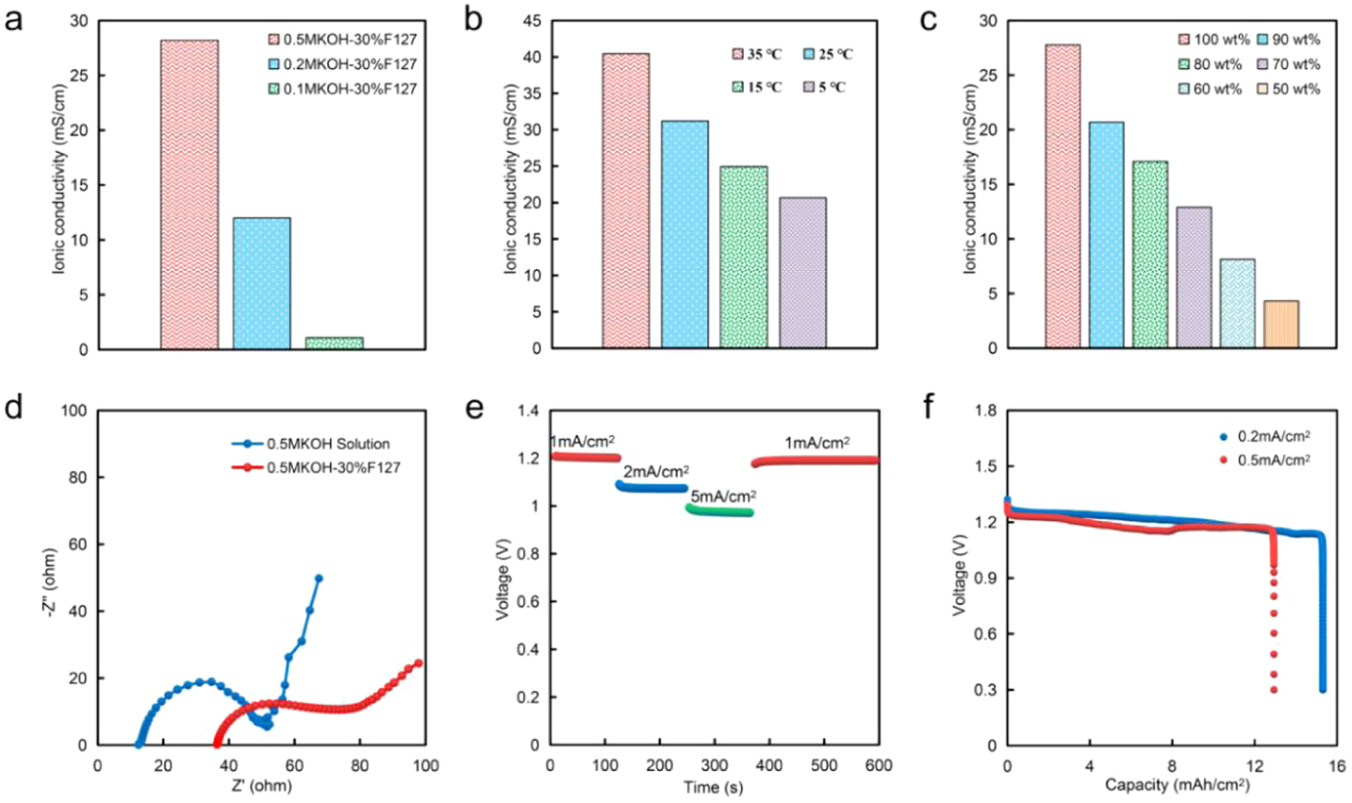

Figure 3. (a) Ionic conductivity of APSE and 30 wt % Pluronic F127 with 0.1 and 0.2 M KOH. (b) Ionic conductivity of APSE at different temperatures of 5, 15, 25, and 35 °C. (c) Ionic conductivity of APSE with different water contents. (d) AC impedance spectra of APSE-based ZAB and 0.5 M aqueous KOH-based ZAB in the frequency range of 100 kHz to 0.01 Hz. (e) Discharge voltage plateau of APSE-based ZAB at different current densities of 1, 2, and 5 mA/cm^2. (f) Discharge curves of APSE-based ZAB at various current densities of 0.2 and 0.5 mA/cm^2.

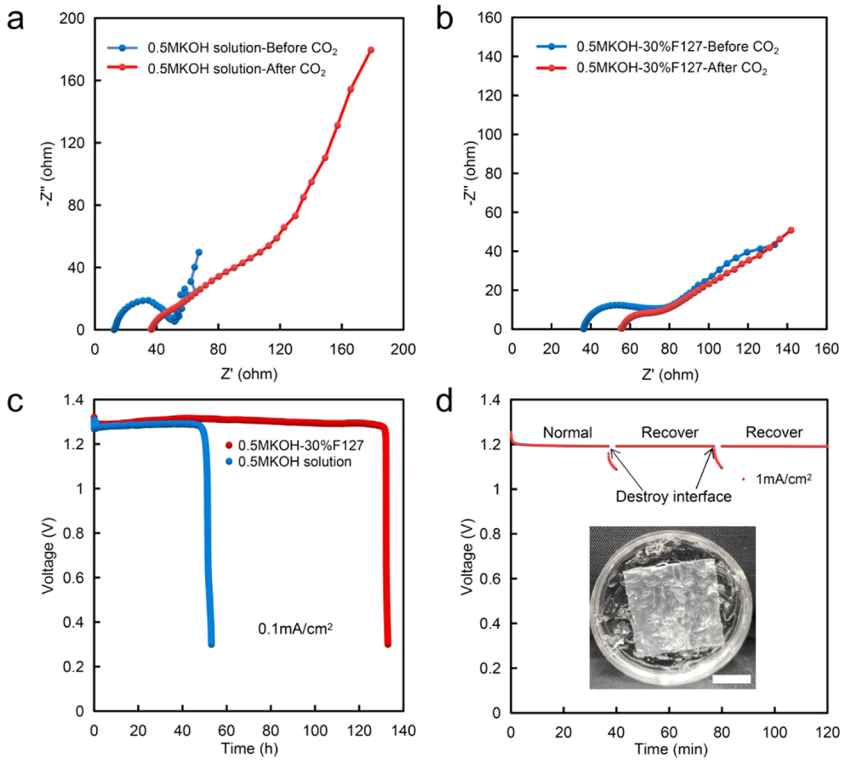

Figure 4. (a) AC impedance spectra of the 0.5 M aqueous KOH-based ZAB before and after CO_2 corrosion in the frequency range of 100 kHz to 0.01 Hz. (b) AC impedance spectra of the APSE-based ZAB before and after CO_2 corrosion in the frequency range of 100 kHz to 0.01 Hz. (c) Discharge curves of APSE-based ZAB and 0.5 M aqueous KOH-based ZAB at a current density of 0.1 mA/cm^2. (d) Self-healing property is shown in the discharge curve of APSE-based ZAB at a current density of 1 mA/cm^2. The destroyed electrolyte/electrode interface is shown in the inset photograph. Scale bar: 1 cm.

is sufficient to render APSE transforming into a liquid and refresh APSE itself, which simultaneously results in a new electrolyte/electrode interface with conformal contact (Figure S2). Consequently, the battery will recover its function without any degradation at room temperature.

To acquire a better understanding of the physicochemical properties of APSE, Fourier transform infrared (FTIR) and X-ray diffraction (XRD) analyses were conducted. In the FTIR spectra, peaks emerging at 1084 and 946 cm^{-1} indicated the C−O−C and C−OH stretch within F127 (Figure 2a). No obvious difference was observed between 30 wt % F127 and APSE, demonstrating that the addition of 0.5 M KOH solution induced no changes in the chemical structure and the sol−gel transition ability of 30 wt % F127. As shown in Figure 2b, no distinct peak was detected from XRD results, proving the amorphous gel state of 30 wt % F127 and APSE. The rheology test showed the storage modulus (G') was significantly higher than the loss modulus (G'') in both 30 wt % F127 and APSE, further exhibiting a gel-state behavior of the samples (Figure 2c).[24] Moreover, the observed high G' manifested the elastic property of APSE, ensuring the flexibility of the fabricated ZABs (Figure 2c).[24] The hydrogel system can readily suffer from evaporation, especially in the semiopen ZAB system during the long discharging process, leading to a decrease in ionic conductivity and the battery failed eventually.[25] Regarding this concern, we examined the water retention capacity of APSE by measuring weight changes over time. Notably, the APSE could hold over 80 wt % water content after 144 h at 25 °C and a relative humidity (RH) of 40% (Figure 2d), thus guaranteeing a high water content during the overall discharge operation (133 h) of the fabricated ZAB (Figure 4c). In the future, additives (e.g., LiCl, CH_3COOK, and $MgCl_2$) may be used in APSE to further enhance its water retention capacity.[26]

To achieve APSE-based flexible ZAB, the ionic conductivity of APSE with various KOH concentrations was investigated as shown in Figure 3a. The ionic conductivity of the optimized APSE showed a conductivity of 29 mS/cm, significantly higher than that with a lower KOH concentration (0.1 M for 1.1 mS/cm and 0.2 M for 12 mS/cm) and some other conventional polymer electrolytes (~1 mS/cm).[27,28] Also, the open-circuit voltage of our ZAB reached over 1.3 V (Figure S3), very close to that of conventional ZAB with 6 M KOH aqueous electrolyte.[29] Furthermore, as the temperature can be a critical factor affecting the ionic conductivity of electrolytes,[30] we also tested the ionic conductivity of APSE under different temperatures. As shown in Figure 3b, the ionic conductivity decreases by decreasing temperature as expected, while the APSE still retained a high ionic conductivity of 20.7 mS/cm at 5 °C, demonstrating a wide operating range. Figure 3c further demonstrates the effect of water content on the ionic conductivity of APSE. Combining with the APSE water retention curve shown in Figure 2d, it was anticipated that over 80 wt % water content after 144 h could still render APSE a high ionic conductivity. The corresponding AC impedance spectra of the aforementioned ionic conductivity are shown in Figure S4. Figure 3d displays the AC impedance spectra of the ZAB based on 0.5 M KOH aqueous electrolyte and APSE, respectively. From the Nyquist plot, although the solution resistance (R_s) of our APSE was higher than the liquid electrolyte, the diameter of the semicircle indicated that there was no obvious difference in the charge transfer resistance

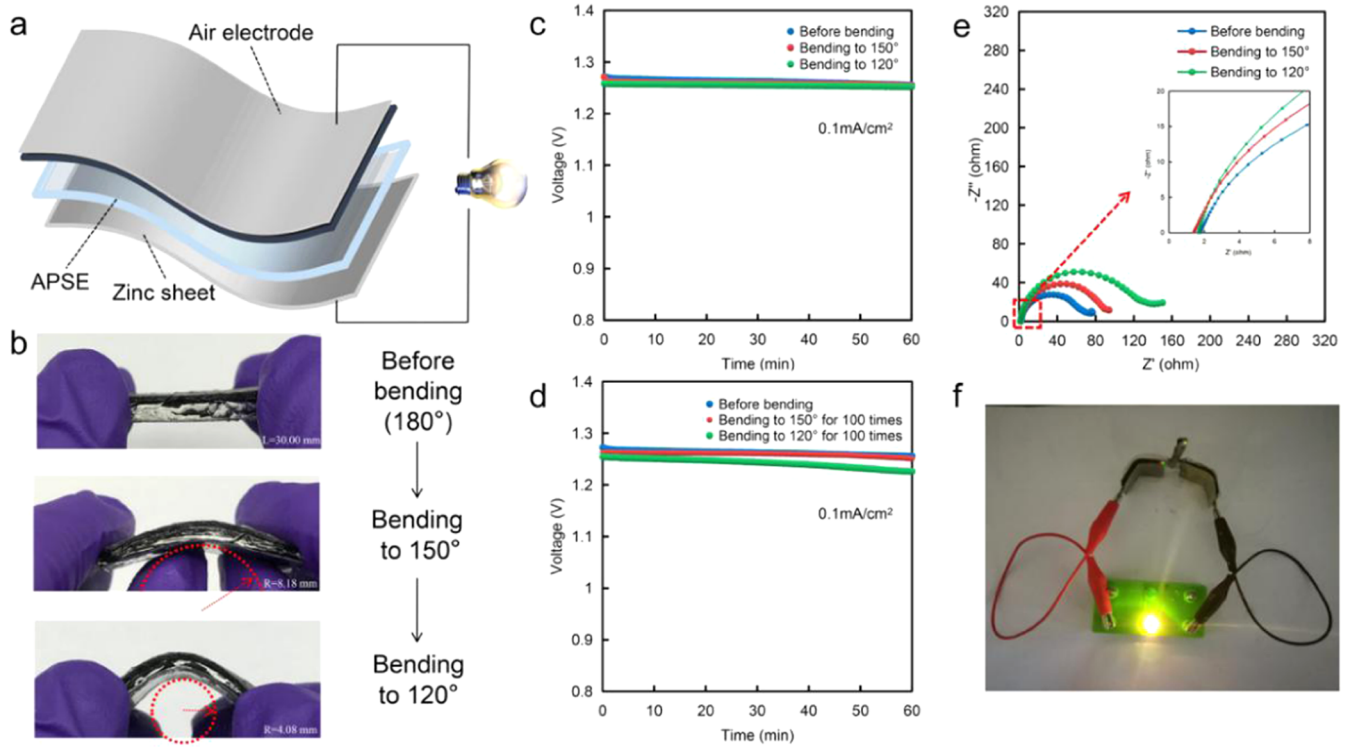

Figure 5. (a) Schematic diagram of APSE-based ZAB. (b) Photographs of the APSE-based ZAB under different bending degrees. (c) Discharge curves of the APSE-based ZAB at a current density of 0.1 mA/cm^2 under flat, 150, and 120° bent states. (d) Discharge curves of the APSE-based ZAB at a current density of 0.1 mA/cm^2 before and after bending to 150 and 120° for 100 times. (e) AC impedance spectra of the APSE-based ZAB under flat, 150, and 120° bent states in the frequency range of 100 kHz to 0.01 Hz. (f) Two 120° bent state APSE-based ZAB connected in series lighting up a 2.5 V light bulb.

(R_{ct}) (Figure S5). This result was partly due to the intimate APSE−electrode contact. The rate performance is displayed in Figure 3e. Despite the solid-state nature and low KOH concentration, our ZAB still exhibited stable and high discharge voltage plateaus under various current densities. As the discharge current density increased from 1 to 5 mA/cm^2, the discharge voltage only decreased by 0.2 V, from 1.2 to 1.0 V. To further investigate the discharge ability of the APSE-based ZAB, galvanostatic discharge measurements were conducted at different current densities (0.2 and 0.5 mA/cm^2) in the ambient environment. As shown in Figure 3f, APSE-based ZAB exhibited a high discharge capacity of 15.3 mA/cm^2 at 0.2 mA/cm^2. Moreover, the cell delivered very close discharge capacity between 0.2 and 0.5 mA/cm^2. The end of discharge showed a rapid drop in voltage, which can be explained by the gradually accumulated zinc oxide (ZnO) passivation layer on the zinc surface.[31] For further validation, we changed the battery components (zinc plate, air electrode, and APSE), respectively, and performed discharge tests again at 0.2 mA/cm^2 after battery failure. As shown in Figure S6, after changing the used air electrode and APSE, the battery showed no discharge capability and the voltage dropped rapidly. However, the battery still discharged stably after changing the used zinc plate. Thus, it could be concluded that the end of discharge was caused by the zinc failure. The formation of the ZnO passivation layer on the zinc surface was mainly due to the decomposition of zincate ions ($Zn(OH)_4^{2-}$) when becoming saturated in APSE.[32] Therefore, though changing the zinc plate, the battery discharge capacity was still shortened because of the $Zn(OH)_4^{2-}$-saturated APSE. After changing both the zinc plate and the APSE, the battery discharge level (voltage) nearly resumed to its initial stage (Figure S6). It is worth mentioning that the air electrode used here was a commercial MnO_2/C electrode, so the ZABs were fabricated as primary cells. Recent progress on designing bifunctional catalysts has significantly improved the power output and rechargeability of ZABs.[33−37] We believe that with systematic design, optimization, and integration, our hydrogel electrolyte may be paired with the state-of-the-art bifunctional electrocatalysts to enable self-healing and anti-CO_2 functions of ZABs, which will be demonstrated using primary ZABs with commercial catalysts as a model system.

For conventional ZAB, carbonation of the electrolyte is inevitable because the CO_2 in the air will diffuse into the battery electrolyte together with O_2 and reacts with the base to form carbonate.[38] Surprisingly, an unprecedented anti-CO_2 property was observed in our APSE-based ZAB. To validate this property, ZABs with 0.5 M KOH liquid electrolyte and APSE were placed in a CO_2-rich environment (a plastic bag full of 2 L of CO_2) for 24 h for allowing sufficient CO_2 diffusion into the battery system and reaction with electrolyte. From Figure 4a,b, the AC impedance spectra showed an obvious difference between the two batteries resulting from their distinct anti-CO_2 ability. After 24 h of CO_2 exposure, not only the R_s value of the liquid-based ZAB tripled but also R_{ct} increased. By comparison, the R_s value of the APSE-based ZAB only increased by half and R_{ct} barely changed (Table S3). To further investigate the CO_2 corrosion tendency, the two batteries were then placed in a 2 L plastic bag with 20% CO_2 for open-circuit voltage (OCV) test (Figure S7). Surprisingly, the OCV of the two batteries both slightly increased under the CO_2-rich (20%) environment compared with that in the

ambient air. However, the OCV of ZAB with 0.5 M KOH solution gradually decreased due to the CO_2 corrosion and the battery failed after 24 h, while the APSE-based ZAB maintained its OCV for over 166 h. Notably, the APSE-based ZAB showed almost 2.5 times discharge duration than that of the liquid-based ZAB, which is reasonable due to the fact that CO_2 can be easily absorbed by traditional alkaline solution.[39] In particular, the voltage plateau of the APSE-based ZAB is slightly higher than that of liquid-based ZAB, showing 1.3 V. The exceptional anti-CO_2 property of APSE can be explained by its higher viscosity compared with 0.5 M KOH solution at 20 °C (~10^7 times greater than that of 0.5 M KOH solution).[21,40,41] Tan et al. have found that in the aqueous solutions with higher viscosity, the diffusion coefficient of CO_2 decreases.[42] Therefore, it is reasonable to explain that APSE with higher viscosity can effectively block the CO_2 diffusion, thus showing a unique anti-CO_2 property.[43] Besides, it is noteworthy that the high viscosity of APSE will not affect the oxygen reduction reaction (ORR) since the O_2 gas will first be reduced to OH^- by the catalysis in the air electrode and then enter APSE as the ion state.[32] In the enriched CO_2 atmosphere, an opaque layer adjacent to air electrode was detected (Figure S8). To figure out the chemical identity of the opaque layer, FTIR and XRD analyses of the initial APSE and the opaque layer were conducted. It was found that the peaks of these two in the FTIR spectra corresponded well with each other and no distinct peak appeared in the XRD spectra, indicating that the composition and the amorphous-state structure of the APSE were not changed (Figure S9). Besides, we placed the APSE in a N_2-protected atmosphere for 48 h to eliminate the interference of CO_2. The photographs also showed that there was a thin opaque layer forming on the N_2-exposure side (Figure S10). Moreover, the weight retention of the APSE is about 88.3% after the N_2 exposure, which agrees well with the result of the water retention test. Thus, we can conclude that the formation of the opaque layer is caused by the water loss of the originally transparent APSE rather than direct reaction with CO_2. In addition, the opaque layer with a higher Pluronic F127 concentration than the transparent APSE will have higher viscosity; hence, it could further prevent CO_2 diffusion in APSE.[21] By comparison, the color of the liquid KOH electrolyte also changed (Figure S11), which is consistent with the previous study.[44] The anti-CO_2 property of APSE effectively elongates the lifetime of ZAB. It is also anticipated that in the future study of ZABs with liquid electrolyte, an anti-CO_2 hydrogel like APSE may be used as an anti-CO_2 electrolyte/air electrode interface to prevent or slow down the carbonation of the alkaline aqueous electrolyte.

On the other hand, to study the self-healing ability of APSE, both APSE−anode and APSE−cathode interfaces were destroyed as illustrated in the inset of Figure 4d. After the deformation of interfaces, the battery voltage gradually declined because of the corresponding decrease in the actual reaction area. Nevertheless, through a simple cooling-recovery process to restore the damaged interface, our battery recovered its original voltage plateau without any loss (Figure 4d).

Figure 5a shows the schematic diagram of the APSE-based ZAB. Supported by a flexible zinc sheet, a commercial MnO_2/C air electrode, and our APSE, the ZAB can be bent to different degrees (150 and 120°) without any visible damages (Figure 5b). With an original length of 30 mm, the corresponding bending radius of the ZAB is 8.18 mm at 150° bending and 4.08 mm at 120° bending, respectively (Figure 5b). Figure 5c,d compares the battery discharge performance under flat (180°) and bent (150 and 120°) states at 0.1 mA/cm^2. Figure 5c verifies that bending to 150 and 120° did not harm the battery discharge performance. Even after repeating bending 100 times from flat to 150 and 120°, the ZAB remained a high-voltage plateau close to that of the flat state (Figure 5d). Moreover, the AC impedance spectra further validate that bending hardly exerts influence on the APSE-based ZAB (Figure 5e). To confirm the practical application of our battery, two of which bent to 120° are connected in series to illuminate a 2.5 V light bulb, as shown in Figure 5f.

CONCLUSIONS

In summary, we have developed a self-healable alkaline hydrogel electrolyte for flexible solid-state ZABs. Through a simple cooling process, the electrolyte exhibits a conformal contact with electrodes and the damaged ZAB recovers to its original state without any performance degradation. Furthermore, the unprecedentedly anti-CO_2 property of the electrolyte significantly elongates the discharge time of ZAB when operated under ambient conditions. It is believed that our new flexible solid-state ZAB has a great potential to power wearable electronics in the future.

EXPERIMENTAL SECTION

Materials. Potassium hydroxide (ACS reagent, 85%, pellets) and Pluronic F127 (PEO_{100}−PPO_{65}−PEO_{100}, critical micelle concentration (CMC):[45] 950−1000 ppm, powder) used in the preparation of APSE were purchased from Sigma-Aldrich without further purification. Zinc electrode (thickness, 0.2 mm) and air electrode (prepared by compressing MnO_2, active carbon, and poly(tetrafluoroethylene) (PTFE) at a weight ratio of 7:2:1 onto nickel foam) were bought from Changsha Spring Energy Corporation. Deionized water was used throughout the experiments.

Preparation of APSE. At room temperature, Pluronic F127 powders with different mass ratios were added into KOH solution with various concentrations in sealed glass vials. To obtain transparent APSE, the F127-KOH suspensions were placed in a −10 °C environment for 30 min and then mixed by a glass bar manually for 30 s. This cooling and mixing step was conducted several times until F127 powders completely dissolved in KOH solution.

Characterization and Electrochemical Detection. The sol−gel transition temperature was measured by an electronic thermometer (Honeywell). The contact angle test was conducted by a digital microscope (Keyence VHX). A scanning electron microscope (SEM, HITACHI, S-4800) was used to observe the cross section of the electrolyte/electrode interface. The FTIR spectra were obtained by a PerkinElmer Spectrum Two FTIR spectrometer (PerkinElmer, Waltham, MA) were used in the attenuated total internal reflection (ATR) mode for spectroscopic analyses of the hydrogel samples. The wavelength resolution was set to 0.5 cm^{-1}. All scans were recorded from 3500 to 500 cm^{-1}. XRD was tested using a Rigaku SmartLab (Japan) in the range of 5−75°. The rheological properties of the hydrogel were tested using a rheometer (TA Instruments, Inc., AR-G2) with a 20 mm plates geometry. The pre-gel ink was injected between geometry and sample stage. The geometry was moving down until reaching a 1000 μm spacing to the sample stage. By default, all tests were performed at T_{stage} = 25 °C and angular frequency was maintained at 6.283 rad/s. To obtain the ionic conductivity of the APSE, the hydrogel electrolyte was placed between two stainless steel sheets over the frequency range of 0.01−100 000 Hz with a magnitude of 10 mV (at OCV). The resistance R (Ω) of the hydrogel with area S (cm^2) and thickness h (cm) was the value of the intersection of the curve at the real part. The ionic conductivity can be calculated as $h/(R \times S)$. Also, the AC impedance spectra of ZAB were measured in the frequency range of 0.01−100 000 Hz with a magnitude of 10 mV (at OCV). The distance

between two electrodes and the volume of APSE and KOH liquid electrolyte are identical in the AC impedance testing of ZABs. The above impedance tests were conducted by a Biologic SP-200 potentiostat and electrochemical workstation (CHI660E). The galvanostatic charge measurements of the ZAB were carried out by a Neware battery testing system. For the water retention capacity evaluation, APSE was placed in the battery test model (an area of 3.14 cm^2 and a height of 19 mm) without any coverage at 25 °C and a relative humidity (RH) of 40%. The weight change rate was calculated by $W_{certain\ time}/W_{initial}$.

CO_2 Exposure. ZABs with APSE and liquid KOH were placed in a 2 L plastic bag full of CO_2, the number of moles of which is about 30 times that of KOH. After CO_2 exposure for 24 h, AC impedance spectra measurements were conducted.

Electrolyte/Electrode Interface Deformation. At room temperature, the APSE-based ZAB (fabricated by a battery test model) was taken apart and the electrolyte/electrode interface was mechanically destroyed by a magnetic stir bar under stirring. Therefore, the intact electrolyte/electrode interface became irregular and loose, leading to a decrease in the actual reaction area. Then, the destroyed battery was reassembled and a discharge test was conducted. After placing the battery in a freezer (−10 °C) for 30 min to restore the damaged interface, the battery was kept in an ambient environment for 30 min for the APSE to return to the intact hydrogel state. A battery discharge test was then performed, and the discharge current density was 1 mA/cm^2.

■ ASSOCIATED CONTENT

Supporting Information

The Supporting Information is available free of charge at https://pubs.acs.org/doi/10.1021/acsami.1c00012.

Optic images of APSE, opaque layer, APSE-based ZAB's voltage, and 0.5 M KOH solutions before and after discharging; schematic figures of the equivalent circuit for fitting EIS spectra; SEM images of the electrode/electrolyte interface; AC impedance spectra of APSE; discharge curves of the APSE-based ZAB before and after changing battery components; OCV curves of the APSE-based ZAB and 0.5 M KOH solution-based ZAB under CO_2 environment; FTIR and XRD patterns of APSE and the opaque layer; sol−gel transition temperature of the APSE; and the EIS fitting values (PDF)

■ AUTHOR INFORMATION

Corresponding Authors

Zheng Chen − *Department of NanoEngineering, Program of Chemical Engineering, and Sustainable Power and Energy Center (SPEC), University of California San Diego, La Jolla, California 92093, United States;* orcid.org/0000-0002-9186-4298; Email: zhengchen@eng.ucsd.edu

Jinhye Bae − *Department of NanoEngineering, Program of Chemical Engineering, Sustainable Power and Energy Center (SPEC), and Materials Science and Engineering Program, University of California San Diego, La Jolla, California 92093, United States;* orcid.org/0000-0002-2536-069X; Email: j3bae@ucsd.edu

Authors

Siyuan Zhao − *Department of NanoEngineering, University of California San Diego, La Jolla, California 92093, United States; School of Mechanical Engineering, Beijing Institute of Technology, Beijing 100081, China; State Key Laboratory of Automotive Safety and Energy, Tsinghua University, Beijing 100084, China*

Dawei Xia − *Department of NanoEngineering, University of California San Diego, La Jolla, California 92093, United States;* orcid.org/0000-0003-4265-2528

Minghao Li − *Materials Science and Engineering Program, University of California San Diego, La Jolla, California 92093, United States*

Diyi Cheng − *Department of NanoEngineering, University of California San Diego, La Jolla, California 92093, United States*

Keliang Wang − *School of Mechanical Engineering, Beijing Institute of Technology, Beijing 100081, China; State Key Laboratory of Automotive Safety and Energy, Tsinghua University, Beijing 100084, China;* orcid.org/0000-0001-6674-3032

Ying Shirley Meng − *Department of NanoEngineering and Sustainable Power and Energy Center (SPEC), University of California San Diego, La Jolla, California 92093, United States;* orcid.org/0000-0001-8936-8845

Complete contact information is available at: https://pubs.acs.org/10.1021/acsami.1c00012

Author Contributions

J.B., Z.C., and S.Z. conceived the idea. S.Z. performed most of the experimental work and prepared the first draft of the manuscript. J.B. and Z.C. directed the project and revised the manuscript. D.X. conducted the mechanical test. M.L. performed the FTIR, SEM characterization, and modulus test. D.C. conducted the ionic conductivity and XRD tests. All authors discussed the results and commented on the manuscript.

Notes

The authors declare the following competing financial interest(s): A patent was filed for this work through the UCSD Office of Innovation and Commercialization.

■ ACKNOWLEDGMENTS

J.B. and Z.C. acknowledge the start-up fund from Jacob School of Engineering at UCSD. This work was performed in part at the San Diego Nanotechnology Infrastructure (SDNI) of UCSD, a member of the National Nanotechnology Coordinated Infrastructure, which is supported by the National Science Foundation (Grant ECCS-1542148). S.Z. and K.W. acknowledge the support by National Natural Science Foundation of China (21706013) and the State Key Laboratory of Automotive Safety and Energy under Project No. KF2024. D.C and Y.S.M. acknowledge partial support from Zable Endowed Chair fund.

■ REFERENCES

(1) Zeng, X.; Hao, J.; Wang, Z.; Mao, J.; Guo, Z. Recent Progress and Perspectives on Aqueous Zn-Based Rechargeable Batteries with Mild Aqueous Electrolytes. *Energy Storage Mater.* **2019**, *20*, 410−437.

(2) Wang, Z.; Li, H.; Tang, Z.; Liu, Z.; Ruan, Z.; Ma, L.; Yang, Q.; Wang, D.; Zhi, C. Hydrogel Electrolytes for Flexible Aqueous Energy Storage Devices. *Adv. Funct. Mater.* **2018**, *28*, No. 1804560.

(3) Liu, Q.; Chang, Z.; Li, Z.; Zhang, X. Flexible Metal-Air Batteries: Progress, Challenges, and Perspectives. *Small Methods* **2018**, *2*, No. 1700231.

(4) Lee, J.-S.; Tai Kim, S.; Cao, R.; Choi, N.-S.; Liu, M.; Lee, K. T.; Cho, J. Metal-Air Batteries with High Energy Density: Li-Air versus Zn-Air. *Adv. Energy Mater.* **2011**, *1*, 34−50.

(5) Wang, K.; Pei, P.; Wang, Y.; Liao, C.; Wang, W.; Huang, S. Advanced Rechargeable Zinc-Air Battery with Parameter Optimization. *Appl. Energy* **2018**, *225*, 848−856.
(6) Qu, S.; Song, Z.; Liu, J.; Li, Y.; Kou, Y.; Ma, C.; Han, X.; Deng, Y.; Zhao, N.; Hu, W.; Zhong, C. Electrochemical Approach to Prepare Integrated Air Electrodes for Highly Stretchable Zinc-Air Battery Array with Tunable Output Voltage and Current for Wearable Electronics. *Nano Energy* **2017**, *39*, 101−110.
(7) Fu, J.; Lee, D. U.; Hassan, F. M.; Yang, L.; Bai, Z.; Park, M. G.; Chen, Z. Flexible High-Energy Polymer-Electrolyte-Based Rechargeable Zinc-Air Batteries. *Adv. Mater.* **2015**, *27*, 5617−5622.
(8) Li, Y.; Fu, J.; Zhong, C.; Wu, T.; Chen, Z.; Hu, W.; Amine, K.; Lu, J. Recent Advances in Flexible Zinc-Based Rechargeable Batteries. *Adv. Energy Mater.* **2019**, *9*, No. 1970001.
(9) Huang, Y.; Li, Z.; Pei, Z.; Liu, Z.; Li, H.; Zhu, M.; Fan, J.; Dai, Q.; Zhang, M.; Dai, L.; Zhi, C. Solid-State Rechargeable Zn//NiCo and Zn-Air Batteries with Ultralong Lifetime and High Capacity: The Role of a Sodium Polyacrylate Hydrogel Electrolyte. *Adv. Energy Mater.* **2018**, *8*, No. 1802288.
(10) Ma, L.; Chen, S.; Wang, D.; Yang, Q.; Mo, F.; Liang, G.; Li, N.; Zhang, H.; Zapien, J. A.; Zhi, C. Super-Stretchable Zinc-Air Batteries Based on an Alkaline-Tolerant Dual-Network Hydrogel Electrolyte. *Adv. Energy Mater.* **2019**, *9*, No. 1803046.
(11) Xu, Y.; Zhang, Y.; Guo, Z.; Ren, J.; Wang, Y.; Peng, H. Flexible, Stretchable, and Rechargeable Fiber-Shaped Zinc-Air Battery Based on Cross-Stacked Carbon Nanotube Sheets. *Angew. Chem.* **2015**, *127*, 15610−15614.
(12) Zhang, J.; Fu, J.; Song, X.; Jiang, G.; Zarrin, H.; Xu, P.; Li, K.; Yu, A.; Chen, Z. Laminated Cross-Linked Nanocellulose/Graphene Oxide Electrolyte for Flexible Rechargeable Zinc-Air Batteries. *Adv. Energy Mater.* **2016**, *6*, No. 1600476.
(13) Fu, J.; Zhang, J.; Song, X.; Zarrin, H.; Tian, X.; Qiao, J.; Rasen, L.; Li, K.; Chen, Z. A Flexible Solid-State Electrolyte for Wide-Scale Integration of Rechargeable Zinc−Air Batteries. *Energy Environ. Sci.* **2016**, *9*, 663−670.
(14) Huang, Y.; Liu, J.; Wang, J.; Hu, M.; Mo, F.; Liang, G.; Zhi, C. An Intrinsically Self-Healing NiCol|Zn Rechargeable Battery with a Self-Healable Ferric-Ion-Crosslinking Sodium Polyacrylate Hydrogel Electrolyte. *Angew. Chem., Int. Ed.* **2018**, *57*, 9810−9813.
(15) Huang, S.; Wan, F.; Bi, S.; Zhu, J.; Niu, Z.; Chen, J. A Self-Healing Integrated All-in-One Zinc-Ion Battery. *Angew. Chem., Int. Ed.* **2019**, *58*, 4313−4317.
(16) Pei, P.; Wang, K.; Ma, Z. Technologies for Extending Zinc−Air Battery's Cyclelife: A Review. *Appl. Energy* **2014**, *128*, 315−324.
(17) Kim, J. G.; Son, B.; Mukherjee, S.; Schuppert, N.; Bates, A.; Kwon, O.; Choi, M. J.; Chung, H. Y.; Park, S. A Review of Lithium and Non-Lithium Based Solid State Batteries. *J. Power Sources* **2015**, *282*, 299−322.
(18) Jeong, B.; Kim, S. W.; Bae, Y. H. Thermosensitive Sol−Gel Reversible Hydrogels. *Adv. Drug Delivery Rev.* **2012**, *64*, 154−162.
(19) Li, L.; Lim, L. H.; Wang, Q.; Jiang, S. P. Thermoreversible Micellization and Gelation of a Blend of Pluronic Polymers. *Polymer* **2008**, *49*, 1952−1960.
(20) Soni, S. S.; Fadadu, K. B.; Gibaud, A. Ionic Conductivity through Thermoresponsive Polymer Gel: Ordering Matters. *Langmuir* **2012**, *28*, 751−756.
(21) Zhao, J.; Sonigara, K. K.; Li, J.; Zhang, J.; Chen, B.; Zhang, J.; Soni, S. S.; Zhou, X.; Cui, G.; Chen, L. A Smart Flexible Zinc Battery with Cooling Recovery Ability. *Angew. Chem., Int. Ed.* **2017**, *56*, 7871−7875.
(22) Linse, P.; Malmsten, M. Temperature-Dependent Micellization in Aqueous Block Copolymer Solutions. *Macromolecules* **1992**, *25*, 5434−5439.
(23) Mainar, A. R.; Iruin, E.; Colmenares, L. C.; Kvasha, A.; de Meatza, I.; Bengoechea, M.; Leonet, O.; Boyano, I.; Zhang, Z.; Blazquez, J. A. An Overview of Progress in Electrolytes for Secondary Zinc-Air Batteries and Other Storage Systems Based on Zinc. *J. Energy Storage* **2018**, *15*, 304−328.
(24) Shi, Y.; Ha, H.; Al-Sudani, A.; Ellison, C. J.; Yu, G. Thermoplastic Elastomer-Enabled Smart Electrolyte for Thermoresponsive Self-Protection of Electrochemical Energy Storage Devices. *Adv. Mater.* **2016**, *28*, 7921−7928.
(25) Liu, J.; Hu, M.; Wang, J.; Nie, N.; Wang, Y.; Wang, Y.; Zhang, J.; Huang, Y. An Intrinsically 400% Stretchable and 50% Compressible NiCo//Zn Battery. *Nano Energy* **2019**, *58*, 338−346.
(26) Bai, Y.; Chen, B.; Xiang, F.; Zhou, J.; Wang, H.; Suo, Z. Transparent Hydrogel with Enhanced Water Retention Capacity by Introducing Highly Hydratable Salt. *Appl. Phys. Lett.* **2014**, *105*, No. 151903.
(27) Park, J.; Park, M.; Nam, G.; Lee, J. S.; Cho, J. All-Solid-State Cable-Type Flexible Zinc-Air Battery. *Adv. Mater.* **2015**, *27*, 1396−1401.
(28) Mohamad, A. A.; Mohamed, N. S.; Yahya, M. Z. A.; Othman, R.; Ramesh, S.; Alias, Y.; Arof, A. K. Ionic Conductivity Studies of Poly(vinyl alcohol) Alkaline Solid Polymer Electrolyte and its Use in Nickel-Zinc Cells. *Solid State Ionics* **2003**, *156*, 171−177.
(29) Zhao, S.; Wang, K.; Tang, S.; Liu, X.; Peng, K.; Xiao, Y.; Chen, Y. A New Solid-State Zinc−Air Battery for Fast Charge. *Energy Technol.* **2020**, *8*, No. 1901229.
(30) Mo, F.; Liang, G.; Meng, Q.; Liu, Z.; Li, H.; Fan, J.; Zhi, C. A Flexible Rechargeable Aqueous Zinc Manganese-Dioxide Battery Working at -20 °C. *Energy Environ. Sci.* **2019**, *12*, 706−715.
(31) Shang, W.; Yu, W.; Liu, Y.; Li, R.; Dai, Y.; Cheng, C.; Tan, P.; Ni, M. Rechargeable Alkaline Zinc Batteries: Progress and Challenges. *Energy Storage Mater.* **2020**, *31*, 44−57.
(32) Tan, P.; Chen, B.; Xu, H.; Zhang, H.; Cai, W.; Ni, M.; Liu, M.; Shao, Z. Flexible Zn−and Li−air Batteries: Recent Advances, Challenges, and Future Perspectives. *Energy Environ. Sci.* **2017**, *10*, 2056−2080.
(33) Han, X.; Ling, X.; Wang, Y.; Ma, T.; Zhong, C.; Hu, W.; Deng, Y. Generation of Nanoparticle, Atomic-Cluster, and Single-Atom Cobalt Catalysts from Zeolitic Imidazole Frameworks by Spatial Isolation and Their Use in Zinc−Air Batteries. *Angew. Chem.* **2019**, *131*, 5413−5418.
(34) Han, X.; Ling, X.; Yu, D.; Xie, D.; Li, L.; Peng, S.; Zhong, C.; Zhao, N.; Deng, Y.; Hu, W. Atomically Dispersed Binary Co-Ni Sites in Nitrogen-Doped Hollow Carbon Nanocubes for Reversible Oxygen Reduction and Evolution. *Adv. Mater.* **2019**, *31*, No. 1905622.
(35) Han, X.; Zhang, W.; Ma, X.; Zhong, C.; Zhao, N.; Hu, W.; Deng, Y. Identifying the Activation of Bimetallic Sites in $NiCo_2S_4$@g-C_3N_4-CNT Hybrid Electrocatalysts for Synergistic Oxygen Reduction and Evolution. *Adv. Mater.* **2019**, *31*, No. 1808281.
(36) Tang, K.; Yuan, C.; Xiong, Y.; Hu, H.; Wu, M. Inverse-Opal-Structured Hybrids of N, S-Codoped-Carbon-Confined Co9S8 Nanoparticles as Bifunctional Oxygen Electrocatalyst for on-Chip All-Solid-State Rechargeable Zn-Air Batteries. *Appl. Catal., B* **2020**, *260*, No. 118209.
(37) Cao, Z.; Hu, H.; Wu, M.; Tang, K.; Jiang, T. Planar All-Solid-State Rechargeable Zn−Air Batteries for Compact Wearable Energy Storage. *J. Mater. Chem. A* **2019**, *7*, 17581−17593.
(38) Cheng, H.-H.; Tan, C.-S. Reduction of CO_2 Concentration in a Zinc/Air Battery by Absorption in a Rotating Packed Bed. *J. Power Sources* **2006**, *162*, 1431−1436.
(39) Cullinane, J. T.; Rochelle, G. T. Kinetics of Carbon Dioxide Absorption into Aqueous Potassium Carbonate and Piperazine. *Ind. Eng. Chem. Res.* **2006**, *45*, 2531−2545.
(40) Kestin, J.; Sokolov, M.; Wakeham, W. A. Viscosity of Liquid Water in the Range -8 °C to 150 °C. *J. Phys. Chem. Ref. Data* **1978**, *7*, 941−948.
(41) Siu, S.; Evans, J. W. Density and Viscosity Measurements of Zincate/KOH Solutions. *J. Electrochem. Soc.* **1997**, *144*, 1278.
(42) Tan, K. K.; Thorpe, R. B. Gas Diffusion into Viscous and Non-Newtonian Liquids. *Chem. Eng. Sci.* **1992**, *47*, 3565−3572.
(43) Xu, N.; Zhang, Y.; Wang, M.; Fan, X.; Zhang, T.; Peng, L.; Zhou, X.; Qiao, J. High-performing Rechargeable/Flexible Zinc-Air Batteries by Coordinated Hierarchical Bi-metallic Electrocatalyst and

Heterostructure Anion Exchange Membrane. *Nano Energy* **2019**, *65*, No. 104021.
(44) Wang, K.; Liao, C.; Wang, W.; Xiao, Y.; Liu, X.; Zhao, S. Physical Shortcut Accelerating Electron Transport of Rechargeable Zinc-Air Battery. *Mater. Today Energy* **2019**, *14*, No. 100340.
(45) Leibler, L.; Orland, H.; Wheeler, J. C. Theory of Critical Micelle Concentration for Solutions of Block Copolymers. *J. Chem. Phys.* **1983**, *79*, 3550−3557.